Hemodynamic Analysis for Cognitive Load Assessment and Classification in Motor Learning Tasks Using Type-2 Fuzzy Sets

Lidia Ghosh, Amit Konar, Pratyusha Rakshit, and Atulya K. Nagar

***Abstract*— The paper addresses a novel approach to assess and classify the cognitive load of subjects from their hemodynamic response while engaged in motor learning tasks, such as vehicle-driving. A set of complex motor-activity-learning stimuli for braking, steering-control and acceleration is prepared to experimentally measure and classify the cognitive load of the car-drivers in three distinct classes: High, Medium and Low. New models of General and Interval Type-2 Fuzzy classifiers are proposed to reduce the scope of uncertainty in cognitive load classification due to the fluctuation of the hemodynamic features within and across sessions. The proposed classifiers offer high classification accuracy over 96%, leaving behind the traditional type-1/type-2 fuzzy and other standard classifiers. Experiments undertaken also offer a deep biological insight concerning the shift of brain-activations from the orbito-frontal to the ventro-lateral prefrontal cortex during high-to-low transition in cognitive load. Further, the activation of the dorsolateral prefrontal cortex is also reduced during low cognitive load of subjects. The proposed research outcome may directly be utilized to identify driving learners with low cognitive load for difficult motor learning tasks, such as taking a U-turn in a narrow space and motion control on the top of a bridge to avoid possible collision with the car ahead.**

***Index Terms*— fNIRs, Motor learning, Hemodynamic Response, Cognitive load classification, Type-2 Fuzzy classifiers.**

I. INTRODUCTION

Cognitive load refers to the psychological engagement of the working memory (located in the pre-frontal lobe [15]) during participation of the brain in learning, reasoning and/or sensory-motor coordination tasks [4]. This paper aims at classifying the cognitive load in motor learning tasks with special emphasis to driving for its diversity and complexity in motor learning. Driving involves several parameters of traffic and road conditions to accurately determine the necessary actions about steering control, braking and acceleration [1]. Driving learners often face extreme difficulties to accurately learn to execute the necessary control actions in a given traffic situation [1]-[3]. The paper aims at developing a scheme for cognitive load assessment and classification of driving learners for different traffic stimuli, such as bumpers ahead, the front car too close, changes in traffic signals, and the like using the brain activation patterns of the subject. The assessment of cognitive load is required to avoid overloading the subjects (driving learners) with excessive psychological distress, causing mental fatigue and/or trauma. Unfortunately, absolute assessment of cognitive load of different subjects in the same scale is difficult as the brain activation measures have different ranges for different people. However, classification of cognitive load with respect to individual's brain activation levels is a relatively simpler problem. Here, we assess and classify cognitive load in motor learning tasks based on individual subject's brain activation patterns.

In [8], electroencephalography (EEG) based cognitive load classification of vehicle-drivers is reported. There are also traces of work in cognitive learning using functional Magnetic Resonance Imaging (fMRI) [10], [11]. However, the poor spatial resolution of EEG due to its volumetric conductivity [9] and excessive

cost of the fMRI devices prohibit their use for the present application. The functional Near-Infrared Spectroscopy (fNIRs) being a low cost device with acceptable spatial resolution thus has been selected. Additionally, the provisions of mounting commercial low cost fNIRs devices over the forehead region (to avoid the influence of hair in the device-response), coupled with the necessity of the prefrontal region to detect cognitive load [5], [44], provide us an opportunity to use fNIRs for this application. Although there are traces of works on fNIRs based experiments on motor learning/memory [6], [13]-[18], [39]-[40], there is hardly any work on cognitive load analysis of subjects during the motor learning phase.

The fNIRs device measures hemodynamic response (i.e., the oxygenated and deoxygenated blood response) of the brain to infrared input. Our experience of working with cognitive load analysis using fNIRs device [12], [59] reveals that the features of the hemodynamic response vary widely across sessions on a given subject. This variation (in inter-session features) often results in an overlap between the features of neighborhood classes, thereby introducing uncertainty in classification of the cognitive load. Most of the traditional classifiers can tolerate small fluctuations in the feature space almost without any errors in classification. Fuzzy classifier comes into play when the degree of fluctuations is relatively wider. The inherent nonlinearity of the fuzzy encoders (fuzzifiers) [42] reduces the wider fluctuation of the feature space into narrower range of membership space. Type-2 fuzzy sets have shown promising results in uncertainty management in classification tasks in presence of wide fluctuations in feature space [1], [24], [29]. The above works inspired us to handle uncertainty in cognitive load classification of motor learning tasks using type-2 fuzzy sets.

Two common variants of type-2 classifiers are popularly used in the literature. They are Interval Type-2 Fuzzy Set (IT2FS) and General Type-2 Fuzzy Set (GT2FS) induced classifiers. Among IT2FS and GT2FS-induced classifiers, the GT2FS classifier has more degree of freedom to capture intra- and inter-session variations [22], and thus is more appropriate for the present application. IT2FS classifiers, on the other hand, have low computational overhead and thus are more tuned to real time applications than their GT2FS counterpart. We here propose both an IT2FS and a GT2FS classifier to classify cognitive load of the brain during driving into 3 classes: High, Medium (Med.), Low and also determine the measure of the cognitive load in a self- normalized scale: [0, 100].

There exist a few interesting works on type-2 fuzzy set induced pattern classifiers. For example, Saha *et al*. designed 2-layered IT2 as well as GT2 fuzzy neural nets using IT2/GT2 fuzzification, firing strength computation and Nie-Tan type reduction. Das *et al*. proposed an evolving IT2FS classifier by employing metacognitive learning algorithms to determine optimal weights of the classifier [50]. Lin *et al.* proposed a self-organizing IT2 fuzzy Neural Network in [51] by employing structural learning for fuzzy rule generation and parameter learning for the selection of parameters in the fuzzy rules. In [52], Das *et al.* introduced a new model of IT2 fuzzy inference system with an online adaptable and self-adaptive structure for motor imagery brain-machine interfaces. Pratama *et al.* in [29] proposed an evolving type-2 classifier (eT2FS) by introducing learning mechanisms to expand, prune, recall and merge rules to address the summarization capability of IT2FS classifier. Andreu-Perez *et al.* proposed a self-adaptive GT2 fuzzy inference system to incrementally update the parameters of the fuzzy rules in a real-time motor imagery-classification problem to control the navigation of a humanoid robot [37]. In [21], Nguyen *et al.* proposed an interesting technique for IT2FS induced motor imagery classification.

Traditional type-2 fuzzy set induced classifiers usually employ rules with interval type-2 fuzzy propositions in the antecedent and type-1/interval type-2 fuzzy propositions in the consequent [29], [37], [50]-[52]. The classifier rules employed in this paper are designed with IT2/GT2 fuzzy propositions in the antecedent and IT2 fuzzy propositions in the consequent. The intra- and inter-session variations in the hemodynamic responses are accommodated in the construction of type-2 membership functions (MFs) of the antecedent propositions. The interval type-2 class MF in the consequent is designed to satisfy an interval range of the class centroid [7].

In this paper, while employing the IT2FS classifier, we compute the upper and lower strengths of rule *j* at the given measurement point. These firing strengths are then used to determine the class centroid of the consequent IT2 MF and the class of the input measurement point. For GT2FS based classification, we adopt a novel vertical-slice approach [35], where the vertical slices are placed in primary-secondary (u-μ) membership planes for distinct values of the linguistic variables. These vertical-planes are capable of

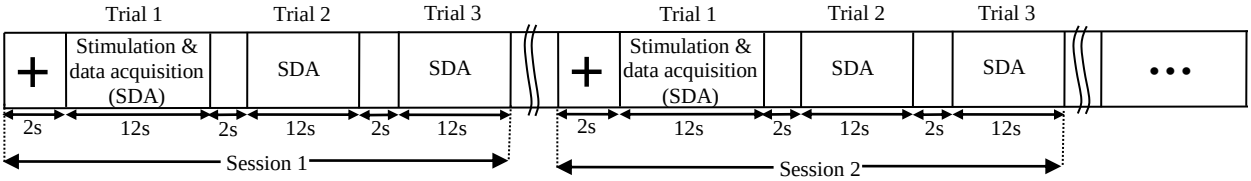

Fig. 1. Defining trial and session for a given subject during offline training

representing the intra- and inter-session related uncertainty at each discrete value of *x*. The vertical-slices are here realized with isosceles triangular MFs, whereas the consequent IT2 MFs of the classifier rules, realized with flat-top approximated triangles, are trapezoidal. Although other functional form of MFs is feasible, triangular vertical slices and class MF are selected for simplicity in representation. We here introduce a novel method to compute firing strength of GT2FS-induced rules at a given measurement point of the linguistic variables. The firing strength is then used to determine the class centroid and hence the class of the input measurement point.

The rest of the paper is structured as follows. Section II provides the principles and methodologies used to pre-process and filter the fNIRs signal. This section also provides an outline to feature extraction, feature selection and training instance generation. Section III deals with the design issues of type-2 fuzzy classifier. Details of experimental set-up along with experiments and results are covered in Section IV. Biological implications are covered in section V. Performance analysis by statistical tests is undertaken in Section VI. Conclusions are summarized in Section VII.

II. Principles and Methodologies

Classification of cognitive load includes five main steps: acquisition and normalization of the fNIRs signals, pre-processing and artifact removal, feature extraction, feature selection and classification. We use the pre-frontal near infra-red imagery to measure the change in concentration of the oxygenated haemoglobin (ΔC_{HbO}) and deoxygenated haemoglobin (ΔC_{HbR}) in each voxel of the fNIRs device. In fNIRs technology, the infrared source-detector connectivity at a specific brain-region is referred to as a voxel. In other words, the response of the brain at a given location at time t can be obtained in terms of $\Delta C_{HbO}(t)$ and $\Delta C_{HbR}(t)$ from a voxel.

A. Normalization of the Raw Data

A cognitive load measurement session contains consecutive *h* trials of fixed duration *T* (=12 seconds) with a time-spacing of 2 seconds between consecutive pairs of the trials (Fig. 1). The duration *T* of a trial is determined by stimulus presentation time, which in turn depends on users' perceiving time, planning time and motor execution time. The sampling rate (*SR*) of the fNIRs device used here is 2 samples/second and is fixed by its hardware. Thus a trial contains $T \times SR = 12 \times 2 = 24$ samples of the fNIRs response. The parameter *h* represents the maximum number of trials in a session for which the brain activation response measured from the onscreen topographic maps [19] remains unaltered. Such adoption in fixation of h is required to measure steady brain activations in different regions of the prefrontal lobe. After experimentation on 37 healthy subjects and 3 patients, we noted that $h = 3$ for healthy (normal) people and $h = 5$ for Alzheimer's patients hold in all cases.

Let $\Delta C_{HbO_\alpha}(t)$ and $\Delta C_{HbR_\alpha}(t)$ be the measure of change in concentrations of *HbO* and *HbR* respectively in mol/litre at voxel α at any time *t* in a session, where $t \in [1, (h \times T \times SR)]$. Let ${}^{Max}\Delta C_{HbO_\alpha}$ and ${}^{Min}\Delta C_{HbR_\alpha}$ be the

maximum and minimum of $\Delta C_{HbO_\alpha}(t)$ and $\Delta C_{HbR_\alpha}(t)$ respectively in a session i.e., for all *t* in [1, (*h* × *T* × *SR*)]. As $\Delta C_{HbO_\alpha}(t) > \Delta C_{HbR_\alpha}(t)$ for all *t*, the difference between $\Delta C_{HbO_\alpha}(t)$ and $\Delta C_{HbR_\alpha}(t)$, representing a measure of *cerebral oxygen exchange* (COE) [26] by the cells in the prefrontal region is normalized in [0, 1] by transformation (1).

$$diff_\alpha(t) = \frac{\Delta C_{HbO_\alpha}(t) - \Delta C_{HbR_\alpha}(t)}{Max\,\Delta C_{HbO_\alpha} - Min\,\Delta C_{HbR_\alpha}} \quad (1)$$

The normalization of $\Delta C_{HbO_\alpha}(t) - \Delta C_{HbR_\alpha}(t)$ is here required to subsequently select uniform support [38] of the MFs irrespective of the sessions. The larger the normalized difference $diff_\alpha(t)$, the higher is the activity of the region, resulting in a higher absorbance of the infrared radiation in that region for carrying relatively more COE than its neighborhood regions [20].

B. Pre-processing

The pre-processing begins with *Common Average Referencing* to eliminate spurious pick-ups due to motion effects. The common average reference signal $CAR_\alpha(t)$ is obtained from $diff_\alpha(t)$ by transformation (2), where $diff_{avg}(t)$ is the average of $diff_\alpha(t)$ over all the voxels in a trial.

$$CAR_\alpha(t) = diff_\alpha(t) - diff_{avg}(t). \quad (2)$$

Here, the $\Delta C_{HbO_\alpha}(t)$, $\Delta C_{HbR_\alpha}(t)$ and the $CAR_\alpha(t)$ are obtained for α = 1 to 16 voxels (brain regions) of the present fNIRs device, covering the entire prefrontal lobe.

In the second stage of pre-processing, we pass the $CAR_\alpha(t)$ signals for α = 1 to 16 voxels through digital *Elliptical band-pass filters* of order 10, where the cut-off frequencies are set to (0.1-3) Hz to remove majority of the physiological artifacts [19] due to eye-blinking (0.5 - 3 Hz) [25], respiration (0.2 - 0.5 Hz), heart-beat (1-1.5 Hz), blood pressure fluctuations or Mayer wave (around 0.1 Hz) [26] etc.

In the third stage, we perform *Independent Component Analysis (ICA)* [27] on $CAR_\alpha(t)$ of 16 voxels to restore the 16 independent components of the hemodynamic response corresponding to 16 voxels of the fNIRs device. The artifact-free 16 ICA components from 16 voxels are then used for subsequent analysis.

C. Feature Extraction

For the sake of feature extraction, we need to extract minute changes on the artifact-free 16 independent components corresponding to 16 voxels. We noted that on an average, the changes in fNIRs response (and so independent component) take place approximately in every 8th sample. So, we divide the 12-second duration (or 24 samples) of a trial into 3 equal time-windows of 4 seconds each. This suffices our requirement. Next we go for extraction of 6 static features [7]: mean (*m*), standard deviation (*sd*), average slope (*s*), skewness (*sk*), kurtosis (*ku*) and average energy (E_{av}) in a time-window. Thus in 3 time-windows, we have 6 × 3 = 18 static features. To take into account of the changes in fNIRs (and hence ICA) response over pairs of consecutive time-windows, we consider the drift in the static features, hereafter referred to as dynamic features [28]. Thus for the transition between 2 consecutive time-windows of 4 seconds each, we have one set of 6 dynamic features. Considering 2 transitions in 3 successive widows, we have altogether 6 × 2 = 12 dynamic features. Consequently, taking static and dynamic features together we have as many as 18 static + 12 dynamic = 30 features for each voxel. Considering 16 voxels, we have 30 × 16 = 480 features for each learning trial.

D. Training Instance Generation for offline Training

Here, we have 3 classes of cognitive load: High, Med. and Low. Given a class, for each subject we prepared 3 sessions per stimulus for a set of 10 stimuli. Again, for each session, we have 3 trials for normal (healthy) subject and 5 trials for brain-diseased subjects. Consequently, for 37 healthy subjects we have 37 × 10 stimuli × 3 session/stimulus × 3 trials/session = 3330 training instances. Again, for 3 brain-diseased subjects, we have 3 × 10 stimuli × 3 session/stimulus × 5 trials/session = 450 training instances. Thus altogether we have 3330 + 450 = 3780 training instances for each class. For 3 classes, we have 3780 × 3 =

11340 training instances [69], each having 480 dimensional features. Although we have 11340 training instances, because of significant inter-subjective variations, we train the classifier with only one subject's training instances at a time. A calculation shown that for each class, we have 10 stimuli × 3 sessions/stimulus × 3 trials/session = 90 training instances per healthy subject and 10 stimuli × 3 sessions/stimulus × 5 trials/session = 150 training instances per brain-diseased subjects.

E. Feature Selection using Evolutionary algorithm

High dimensional features unusually enhance the training time of the classifiers [63]. In addition, because of the possible influence of measurement noise on the features, training with high dimensional features does not often guarantee good classification accuracy in the test phase [64]. Feature selection attempts to optimally select a few independent features from the high dimensional features, capable of sufficiently discriminate the classes (here three classes, representing High, Med. and Low cognitive load). Among the feature selection algorithms, sequential forward selection (SFS) and sequential backward selection (SBS) are well-known in the literature [2]. The SFS (SBS) algorithm iteratively adds (deletes) one feature at a time to an empty (complete) feature set with an aim to select the best m out of M ($>>m$) features. However, SFS/SBS algorithm suffers from one common limitation, called the "nesting effect" [2], which prohibits the deletion (addition) of a feature once added (excluded).

One approach to overcome the nesting effect is to randomly select m out of M features simultaneously by an iterative algorithm with the intent to improve the relative quality of features over the iterations with respect to their ability to discriminate the classes. Evolutionary algorithms (EAs) utilize population-based search of trial solutions in a high dimensional space to obtain an optimal solution of a well-defined objective function for a given problem. In the present context, EAs would provide optimal solution to the feature selection problem, if the search is carried out to find the optimal set of m features that jointly minimize the distance between each pair of points in a class (intra-class separation distance) and maximize the distance between each pair of class centroids (inter-class separation distance).

Let $\vec{x}_i^c = [x_{i,1}^c, ..., x_{i,M}^c]$ be the i^{th} data point, describing a feature vector, falling in class c, where each class c contains P number of data points, i.e., i = 1 to P for c = 1 to N classes. Further, let b_k^c and b_k^d respectively denote the k-th component of the class centroids for class c and d for k = 1 to M. The aim of the proposed evolutionary based feature selection algorithm is to optimally select m out of M features simultaneously to maximize inter-class separation distance and minimize intra-class separation distance. We intuitively design two objective functions (3) and (4) to reduce intra-class separation and enhance inter-class separation. In (3) and (4), we consider city block distance, rather than conventional Euclidean distance to reduce the additional overhead in computing square and square-root in Euclidean distance.

It may be noted that the increase in inter-class separation distance and decrease in intra-class separation distance are no way conflicting [65]. So, we plan to go for single objective, rather than multi-objective (bi-objective) optimization. To formulate the problem in the settings of single objective optimization, we combine (3) and (4) to obtain (5), which needs to be minimized in order to minimize (3) and maximize (4). In (5) one parameter η is introduced to avoid a possible division by zero, particularly when obj_2 assumes a zero value in the denominator in (5). We prefer a small positive value of η to minimally disturb the ratio obj_1/obj_2. For optimal choice of η along with other parameters of the classifiers, we used a meta-heuristic optimization algorithm. The optimal value obtained in the selected range [0.001, 0.5] is 0.0028. Details of selection of η are discussed in the experiment section.

$$obj_1 = \sum_{c=1}^{N} \sum_{i=1}^{P} \sum_{k=1}^{m} | x_{i,k}^c - b_k^c | \tag{3}$$

$$obj_2 = \sum_{\substack{c=1 \\ d \neq c}}^{N} \sum_{d=1}^{N} \sum_{k=1}^{m} | b_k^c - b_k^d | \tag{4}$$

$$obj_3 = \frac{obj_1}{\eta + obj_2} \tag{5}$$

Among the well-known meta-heuristic algorithms, Differential Evolution (DE) algorithm has shown remarkable performance in single-objective multi-modal optimization problems [61]. DE is said to outperform its competitors with respect to its small code-length, a fewer control parameters and low computational overhead [62]. Apart from these, we select it for the present application for our familiarity with it for several years [32], [49]. Although quite a few variants of DE are available, we here employ one of its widely used versions, called DE/rand/1/bin. In this version of DE, we have 3 parameters, the scale factor *F*, the crossover rate *CR* and a uniform population size *NP*. In our realization, both *F* and *CR* are selected as 0.7 and *NP* is selected as 20. The trial solutions (parameter vectors) of length $m = 8$ are used to select 8 best features from a given list of $M = 480$ features.

F. Classifier Training and Testing

Before proceeding for our proposed classifier design we trained a typical Linear Support Vector Machine (LSVM) [55] and a SVM with Radial Basis Function as the kernel (SVM-RBF) [56] classifier. While undertaking training, we set aside 10% of the training instances per class/per subject for subsequent testing. Thus for normal subjects, we have 90% of 90 = 81 training instances/per subject/class, and similarly for brain-patients we have 135 instances/subject/class. After the training is over, we test the classifier performance and we found 99.98% classification accuracy for each class for each subject. Next we go for testing on real instances by instantiation with actual traffic stimuli. It is found that the classifier accuracy falls off drastically to 89% for LSVM and to 92% for SVM-RBF. This inspired us to think of designing a type-2 fuzzy classifier for possible improvement in classification accuracy.

III. CLASSIFIER DESIGN

This section provides a detailed design of IT2FS and GT2FS induced classifiers for classification of cognitive load.

A. Preliminaries on IT2FS and GT2FS

Definition 1: A *classical/type-1 fuzzy set S* [38], defined on the universe of discourse *X* of a linguistic variable *a*, is a two-tuple, given by

$$S = \{(a, \mu_S(a)) \mid \forall a \in X\} \tag{6}$$

where, $\mu_S(a)$ is the membership of *a* in *S*. $\mu_S(a)$ is a crisp number in the closed interval [0, 1] for any $a \in X$.

Definition 2: A *General Type-2 Fuzzy Set* (*GT2FS*) $\tilde{S}$ is a three-tuple [60], given by

$$\tilde{S} = \{a, u_{\tilde{S}}(a), \mu_{\tilde{S}}(a,u)\} \mid a \in X, u(a) \in J_a \subseteq [0,1]\} \tag{7}$$

where, $u_{\tilde{S}}(a)$, known as primary membership, is a crisp number in [0, 1] and $\mu(a,u) \in [0,1]$ is the secondary or type-2 MF.

Definition 3: For a given $a = a'$ the 2D plane comprising u and $\mu_{\tilde{S}}(a',u)$ is referred as *vertical slice* on $\mu_{\tilde{S}}(a,u)$ [35].

Definition 4: For a given universe of discourse *X* of a linguistic variable *a*, if $\mu_{\tilde{S}}(a,u) = 1, \forall a \in X$ and $\forall u \in J_a \subset [0,1],$ then the type-2 fuzzy set $\tilde{S}$ is called an *Interval Type-2 Fuzzy Set* (*IT2FS*) [43].

Definition 5: An IT2FS comprises infinite number of *embedded type-1 fuzzy sets* [43]. Let S_e be an embedded fuzzy set in the IT2FS, then the *Lower MF (LMF)* of an IT2FS is computed as

$$\underline{\mu}_{\tilde{S}}(a) = \underset{\forall e}{Min}\,(\mu_{S_e}(a)), \forall a \tag{8}$$

Similarly the *upper MF* (*UMF*) of an IT2FS is computed as

$$\bar{\mu}_{\tilde{S}}(a) = \underset{\forall e}{Max}(\mu_{S_e}(a)), \forall a \qquad (9)$$

Thus an IT2FS is always bounded by 2 curves: the UMF and the LMF. The bounded region of the IT2FS is called the *Footprint of Uncertainty* (FOU) [43], which is defined by the union of all the embedded type-1 fuzzy sets in an IT2FS.

B. IT2FS Induced Classifier Design

In the present learning problem, we propose a fuzzy classifier using interval type 2 fuzzy sets (IT2FS) [23] to classify the data points with reduced dimension into three classes: High, Med. and Low. Let $x_{i,k}$ be a selected fNIRs feature having *f* experimental instances $x_{1,k}, x_{2,k}, ..., x_{f,k}$ taken on the same day on the same subject. Let the instances of x_k have a mean m_k and variance σ_k. We construct a type-1 isosceles triangular MF with the centre of its base located at $x_k = m_k$ and the two end points of the base located at $x_k = m_k - 3\sigma_k$ and $x_k = m_k + 3\sigma_k$. The peak values of the isosceles triangular MFs are unity to maintain the normality condition. This triangular type-1 MF represents that the instances of x_k are close enough to the mean value of the points and is referred to as $\mu_{CLOSE-to-mean(}(x_k)$, abbreviated as $\mu_C(x_k)$.

Now suppose the experiments are repeated for *s* days (D_1, D_2, …, D_s) on the same subject. Then for *s* days, we would have *s* isosceles triangular MFs $\mu_C^{D_z}(x_k)$ for *z* = 1 to *s*. We take the min and max of these type-1 MFs to obtain the UMF and the LMF [22] of an IT2FS, where

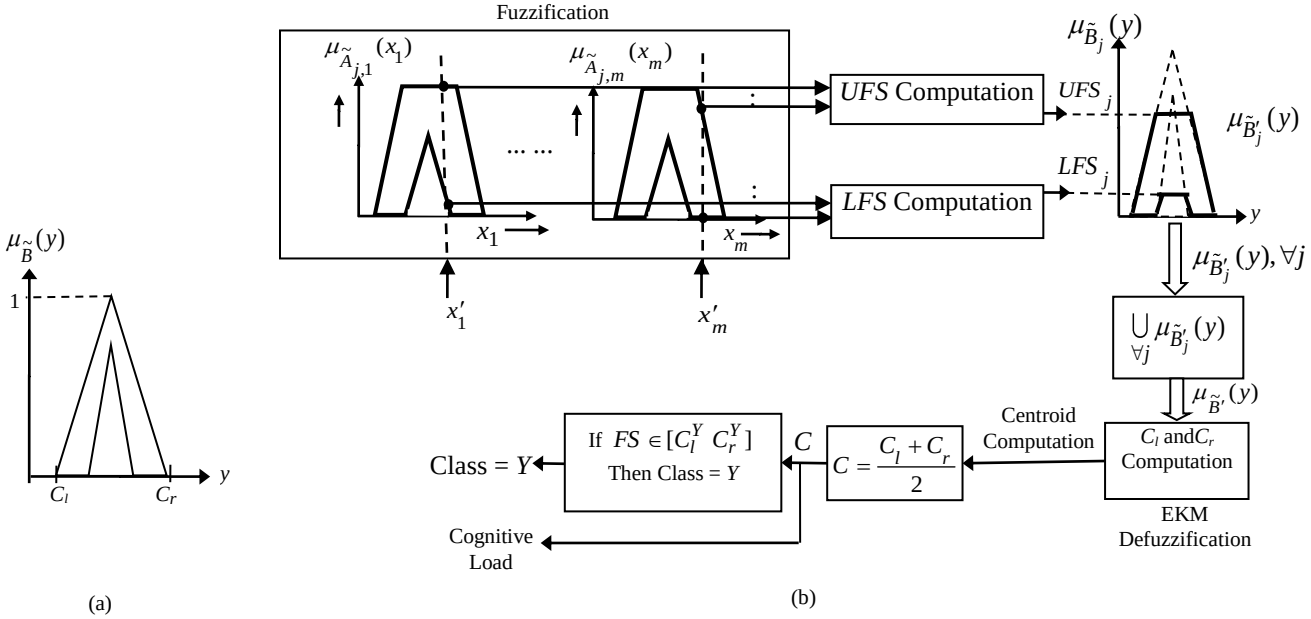

Fig. 3 (a). Consequent type-2 class MF, (b) IT2FS classifier design

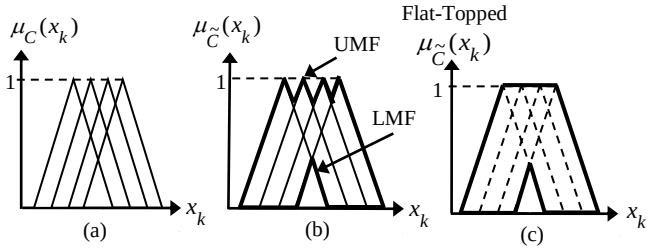

Fig. 2. Construction of Flat-top IT2FS: (a) type-1 MFs, (b) IT2FS representation of (a), (c) flat-top approximated IT2FS

$$UMF(x_k) = \bar{\mu}_{\tilde{C}}(x_k) = \underset{z=1}{\overset{s}{Max}}(\mu_C^{D_z}(x_k)) \qquad (10)$$

$$LMF(x_k) = \underline{\mu}_{\tilde{C}}(x_k) = \underset{z=1}{\overset{s}{Min}}(\mu_C^{D_z}(x_k)) \quad (11)$$

Thus for *m* features, we have *m* IT2FS given by $[\bar{\mu}_{\tilde{C}}(x_k), \underline{\mu}_{\tilde{C}}(x_k)]$, k = 1 to *m*. To ensure convexity of the constructed IT2FS, we go for flat-top approximation [34] of the obtained IT2FS by joining the peaks of the individual type-1 MFs by a straight line of zero slope [33] (Fig. 2(c)).

Type-2 Fuzzy Inference Generation: Consider a set of type-2 classifier rules, where the format of an arbitrary rule *j*, is presented below:

Rule *j*: **IF** x_1 is $\tilde{A}_{j,1}$, x_2 is $\tilde{A}_{j,2}$, ..., x_m is $\tilde{A}_{j,m}$, **THEN** class-centroid *y* of $\mu_{\tilde{B}_j}(y)$ lies in $[C_l^Y \; C_r^Y]$. Here, x_k is a linguistic variable in universe X_k, $\tilde{A}_{j,k}$ is a trapezoidal IT2 MF representing that x_k is CLOSE-to-the-Centre of the support [38] of x_k, for k =1 to *m*; $\mu_{\tilde{B}_j}(y)$ is a isosceles triangular IT2FS (Fig. 3(a)) representing that the class centroid *y* is Close-to-the-Centre of the bases of the UMF and the LMF. The UMF and the LMF of $\mu_{\tilde{B}_j}(y)$ are symmetric around a hypothetical vertical line passing through the centre of the base. Each $\mu_{\tilde{B}_j}(y)$ is associated with an interval $[C_l^Y \; C_r^Y]$, where C_l^Y and C_r^Y are called *the left and the right end point class centroids* [43] of class *Y*, which denote the possible range of the IT2 centroid of the consequent $\mu_{\tilde{B}_j'}(y)$ after firing of the rule *j*. The following considerations are used in the optimal settings of the class boundaries C_l^Y and C_r^Y.

1. The range of possible class centroids of individual classes should not have any overlap.

2. There should not be any spacing between the upper bound of one class centroid and the lower bound of the adjacent class centroid. Here, the 3 class boundaries should be $[C_l^{Low}\ C_r^{Low})$, $[C_r^{Low}\ C_r^{Med})$ and $[C_r^{Med}\ C_r^{High}]$.

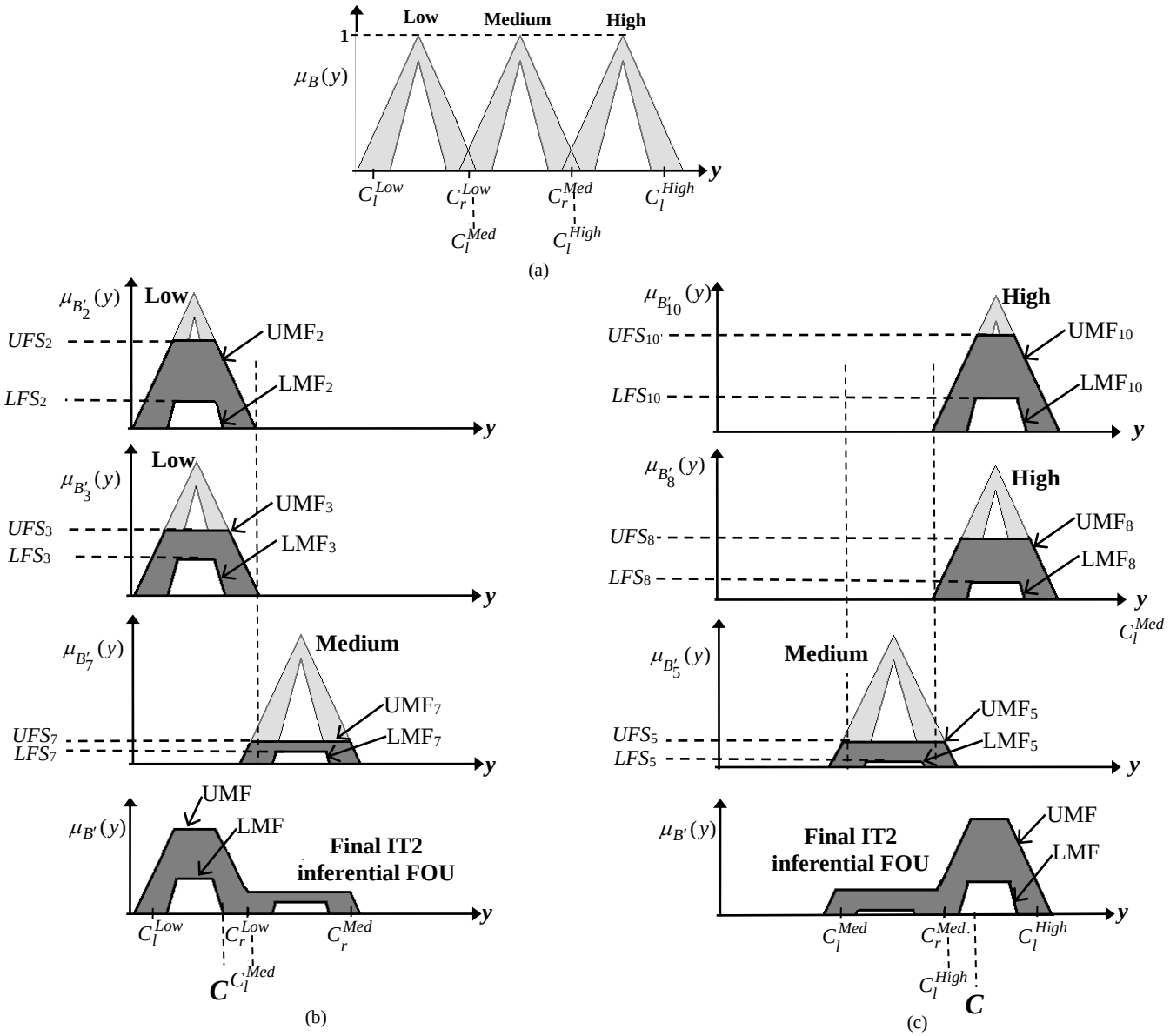

Fig. 4 (a). Consequent IT2 MF for 3 classes: Low, Med. and High cognitive loads with initial class centroid positions , (b) defuzzified output C falls in Low cognitive load class after firing of rule 2, 3 and 7, (c) defuzzified output C falls in High cognitive load class after firing of rule 10, 8 and 5.

3. The optimal setting of $[C_l^Y\ C_r^Y]$ for any class Y should maximize classification and minimize misclassification for each class.
4. The least value of class-centroid of the Low class should be 0, indicating no cognitive load, and the largest value of class-centroid of class High should be 100, indicating maximum cognitive load. In other words, we assign a scale of [0, 100] for the cognitive load.

An evolutionary optimization realized with DE is used here for optimal setting of class boundaries (along with η) satisfying the above criteria. The structure of the IT2FS used for the 3 classes are shown in Fig.4 (a) for convenience.

The $\mu_{\tilde{B}_j}(y)$ is constructed with the centre of its base located at $(C_l^Y + C_r^Y)/2$ and is symmetric around the vertical axis passing through the centre. The UMF of the consequent IT2FS is considered normal (i.e., the peak membership = 1). The LMF of the consequent IT2FS is constructed as a relatively smaller isosceles

triangle with intuitively chosen base-width = 40% of the base-width of the UMF and height = 80% of the height of the UMF. This in other words offers a large tolerance to C_l^Y and C_r^Y to improve classification accuracy.

Let $x_1 = x_1', x_2 = x_2', .., x_m = x_m'$ be a measurement point. We obtain the lower firing strength (LFS_j) and upper firing strength (UFS_j) at the measurement point for rule *j* by (12) and (13).

$$LFS_j = Min(\underline{w}_j, \underset{k=1}{\overset{m}{Min}}(\underline{\mu}_{\tilde{A}_{j,k}}(x_k'))) \tag{12}$$

$$UFS_j = Max(\overline{w}_j, \underset{k=1}{\overset{m}{Min}}(\overline{\mu}_{\tilde{A}_{j,k}}(x_k'))) \tag{13}$$

Here, $\underline{w}_j$ and $\overline{w}_j$, lying in [0, 1], are respectively the upper limit of $\underset{k=1}{\overset{m}{Min}}(\underline{\mu}_{\tilde{A}_{j,k}}(x_k'))$ and lower limit of $\underset{k=1}{\overset{m}{Min}}(\overline{\mu}_{\tilde{A}_{j,k}}(x_k'))$. The introduction of the $\underline{w}_j$ and $\overline{w}_j$ in (12) and (13) provides a mechanism to control the area under the consequent FOU, thereby controlling the location of the centroid of the resulting consequent IT2 MF. The optimal values of $\underline{w}_j$ and $\overline{w}_j$ are determined by an evolutionary algorithm with an aim to maximize the classification accuracy for individual classes. Although any evolutionary algorithm could serve the purpose, we selected the well-known DE algorithm [49] for its simplicity in coding, fewer control parameters and above all our familiarity with the algorithm [32]. The optimal selection of $\underline{w}_j$ and $\overline{w}_j$ is undertaken in the experiment section.

We now compute the consequent IT2 MF $\mu_{\tilde{B}_j'}(y)$ with UMF and LMF obtained by (14) and (15).

$$\overline{\mu}_{\tilde{B}_j'}(y) = Min(\overline{\mu}_{\tilde{B}_j}(y)), UFS_j) \tag{14}$$

$$\underline{\mu}_{\tilde{B}_j'}(y) = Min(\underline{\mu}_{\tilde{B}_j}(y)), LFS_j) \tag{15}$$

In case more than one rule with same or different class labels at the consequent are fired by instantiation of the antecedent linguistic variables, then we obtain the final inference $\tilde{B}'$ by taking union of the individual inference $\tilde{B}_j'$, for all *j*.

$$\tilde{B}' = \bigcup_{\forall j} \tilde{B}_j' = [\bigcup_{\forall j} \underline{\tilde{B}}_j' \quad \bigcup_{\forall j} \overline{\tilde{B}}_j'] \tag{16}$$

Here, $\tilde{B}'$ refers to an IT2FS, whose LMF and UMF are the maximum of the constituent $\tilde{B}_j'$s' LMF and UMF respectively. We next obtain the left and the right end point centroids C_l and C_r respectively of the resulting IT2MF $\tilde{B}'$ by using the well-known *Karnik Mendel (KM) Algorithm* [31], and hence determine the centroid *C* of the resulting IT2Fs using (17). The centroid *C* here represents the cognitive load of the subject.

$$C = \frac{C_l + C_r}{2} \tag{17}$$

The KM algorithm aims at finding the left (right) switch point from the UMF (LMF) to the LMF (UMF) in an iterative manner, such that the centroid of one embedded fuzzy set, following the UMF (LMF) up to the switch point and following the LMF (UMF) after the switch point, is equal to the switch point. The left (right) end switch point is defined as left (right) end point centroid.

Lastly we determine the class *Y* of the input measurement by determining the class interval $[C_l^Y \; C_r^Y]$, that includes the class centroid *C*. Since the class boundaries for each class is non-overlapped and distinct, the class *Y* can be correctly identified, if *C* falls in the above interval. Several extensions to KM algorithm have been reported in the literature with a main motive to reduce computational overhead [66] and to suit real-time applications by approximating in centroid computation [67]. We here used Enhanced KM (EKM) [30] algorithm for its low computational overhead and high popularity.

In Fig. 4, we schematically demonstrate the computation of $\tilde{B}'$ from $\tilde{B}'_j$ for all j, and next show results of computation of C_l and C_r and the centroid C of $\tilde{B}'$ for firing of 2 sets of rules. For the first set of rules, the centroid C is found to lie in $[C_l^{Low}\ C_r^{Low}]$, whereas for the latter set of rules, the centroid falls in $[C_l^{High}\ C_r^{High}]$, indicating Low and High classes as the resulting classifier outputs in Fig. 4(b) and (c) respectively.

C. GT2FS Induced Classifier Design

A GT2FS [35] is a three tuple $< x, u_{\tilde{A}}(x), \mu(x,u) >$, where x is a linguistic variable (here, feature value), $u_{\tilde{A}}(x)$ is the primary MF and $\mu(x,u)$ is the secondary MF. Both the primary and the secondary MFs lie in [0, 1]. Here, we present a GT2FS in vertical slice form [35] (Fig. 5), where each vertical slice represents secondary MF with respect to primary membership at a given $x = x'$, say. Given a GT2FS classifier rule j: **If** x_1 is $\tilde{A}_{j,1}$, x_2 is $\tilde{A}_{j,2}$, ..., x_m is $\tilde{A}_{j,m}$ **Then** class centroid y of $\mu_{\tilde{B}_j}(y)$ lies in $[C_l^Y\ C_r^Y]$. Here, x_k is $\tilde{A}_{j,k}$ for k = 1 to m are GT2FS-induced propositions and $\mu_{\tilde{B}_j}(y)$ denotes an IT2FS consequent MF.

Definition 1: We define the t-norm (denoted by $\overset{t}{\mathrm{X}}$) between two vertical planes $G_p = \mu_{\tilde{A}_{j,p}(x'_p)}(u_{p,l})$ and $G_q = \mu_{\tilde{A}_{j,q}(x'_q)}(u_{q,v})$ of $\tilde{A}_{j,p}$ and $\tilde{A}_{j,q}$ respectively by (18).

$$G_p \overset{t}{\mathrm{X}} G_q = \{\mu_{\tilde{A}_{j,p}(x'_p)}(u_{p,l})\, \mathrm{t}\, \mu_{\tilde{A}_{j,q}(x'_q)}(u_{q,v}) \,|\, l, v \in [1,n]\}. \quad (18)$$

Here, we take t = min. For any three vertical planes G_p, G_q and G_r taken from $\tilde{A}_{j,p}$, $\tilde{A}_{j,q}$ and $\tilde{A}_{j,r}$, the

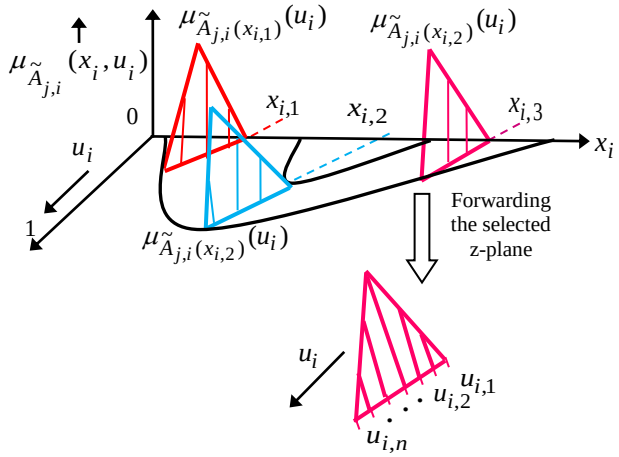

Fig. 5. Secondary Membership Assignment

cumulative t-norm is defined by $G_p \overset{t}{\mathrm{X}} G_q \overset{t}{\mathrm{X}} G_r = (G_p \overset{t}{\mathrm{X}} G_q) \overset{t}{\mathrm{X}} G_r$. In general, the cumulative t-norms of G_1, G_2, … , G_m, taken from m distinct GT2FS, is evaluated in the fixed order of occurrence of G_k, k = 1 to m.

Definition 2: To compute the s-norm between two vertical slices G_p and G_q introduced above, we simply replace t by s in (18), where we take s = max. The cumulative s-norm is computed by replacing t by s (=max) in cumulative t-norm.

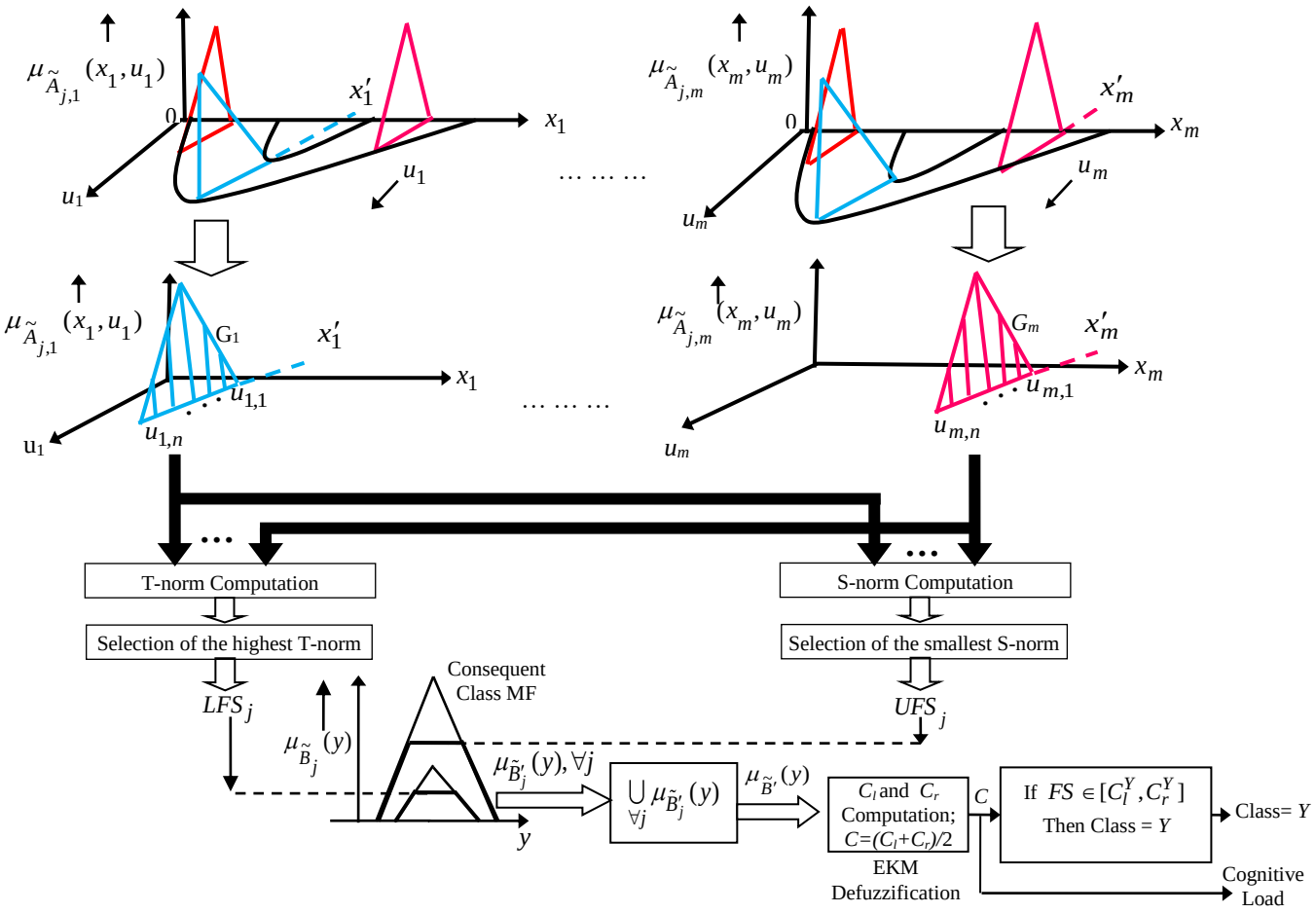

Fig. 6. GT2FS Classifier Design

Given a measurement point: $x_k = x'_k$ for k = 1 to m, we obtain the firing strength of rule j by the following five steps (Fig. 6).

1. Let $G_1 = \mu_{\tilde{A}_{j,1}(x'_1)}(u_1)$, $G_2 = \mu_{\tilde{A}_{j,2}(x'_2)}(u_2)$,…, $G_m = \mu_{\tilde{A}_{j,m}(x'_m)}(u_m)$. We compute $G = G_1 \overset{t}{\times} G_2 \overset{t}{\times} \ldots \overset{t}{\times} G_m$ by (18) to obtain n^m terms in G.
2. We evaluate the largest of the n^m terms in G and call it LFS_j, i.e.,

$$LFS_j = Max\{\mu_{\tilde{A}_{j,1}(x'_1)}(u_1)\, t\, \mu_{\tilde{A}_{j,2}(x'_2)}(u_2)\, t \ldots t\, \mu_{\tilde{A}_{j,m}(x'_m)}(u_m)\} \quad (19)$$

3. Similarly we compute $H = G_1 \overset{s}{\times} G_2 \overset{s}{\times} \ldots \overset{s}{\times} G_m$.
4. We evaluate the smallest of the n^m terms in H and call it UFS_j, i.e.,

$$UFS_j = Min\{\mu_{\tilde{A}_{j,1}(x'_1)}(u_1)\, s\, \mu_{\tilde{A}_{j,2}(x'_2)}(u_2)\, s \ldots s\, \mu_{\tilde{A}_{j,m}(x'_m)}(u_m)\} \quad (20)$$

It can be easily verified that $UFS_j \geq LFS_j$. Further, UFS_j and LFS_j provide the Least Upper bound (LUB) and the Greatest Lower Bound (GLB) of the constituent secondary MFs, each contributed by one vertical plane of *m* antecedent GT2FS.

5. Compute the consequent IT2 MF $\mu_{\tilde{B}'_j}(y)$ with UMF and LMF obtained by (14) and (15).
6. If multiple rules fire for $\tilde{B}_j$, then we need to take the union of all the type-2 inferences as indicated in (16).
7. Next we decode (defuzzify) the type-2 inference class using EKM Defuzzification technique [30] and obtain left and right end point centroids C_l and C_r. We finally evaluate the class centroid *C* by (17).

Now, identify the pre-defined class by defining the class interval $[C_l^Y \; C_r^Y]$, that includes the class centroid *C*. If *C* falls in the above interval, then class = *Y*.

IV. Experiments and Results

A. Experimental Set-up

Experiments are undertaken with a Logitech driving simulator, comprising one steering wheel, one brake and one accelerator foot pedal and a monitor to drive the simulated car (Fig. 7(a)) and an fNIRs device, manufactured by BIOPAC, with 4 infrared (IR) sources and 10 infrared detectors, placed in an array for mounting on the forehead (Fig. 7(b)). The IR sources are triggered by short duration electrical pulses in a time-multiplexed manner to ensure activation of only one source at a time. On triggering of a selected source, the infrared signal penetrates the pre-frontal region below the source, and the received energy is partially absorbed by the brain and partially reflected back to the four detectors mounted around each source (Fig. 7(c)). The sampling rate of the fNIRs device being 2 Hz, the sampling intervals are of 0.5 seconds. The sampling interval constitutes four equal time-slices of 0.125 seconds, where each time-slice is utilized to receive oxygenated (*HbO*) and deoxygenated (*HbR*) blood response (Fig. 7(d)) by one of four detectors around each source. Thus for 4 sources, we obtain 16 oxygenated and 16 deoxygenated blood response of 16 voxels (brain regions) in 0.5 seconds. It is important to note that the penetration depth of the IR signals is 1.25 cm from the surface of the scalp. The signal acquisition is performed using (Cognitive Optical Brain Imaging) COBI studio software, supplied by the manufacturer.

B. Participants

Forty right-handed volunteers (driving learners), in the age group: 20-55 years with normal/corrected vision participated in this experiment. The participants include 37 healthy subjects (20 male and 17 female) and 3 male patients suffering from the Alzheimer's disease.

C. Stimulus Presentation for online classification

During online cognitive load classification, each subject is instructed to perform driving on a selected road map containing multiple occurrences of the 10 stimuli (Table I) in a random order. Each visual stimulus is of 12 seconds duration. The list of stimuli along with the motor actions required in response to the respective stimulus is given in Table-I. The structure of the stimulus is given in Fig. 8.

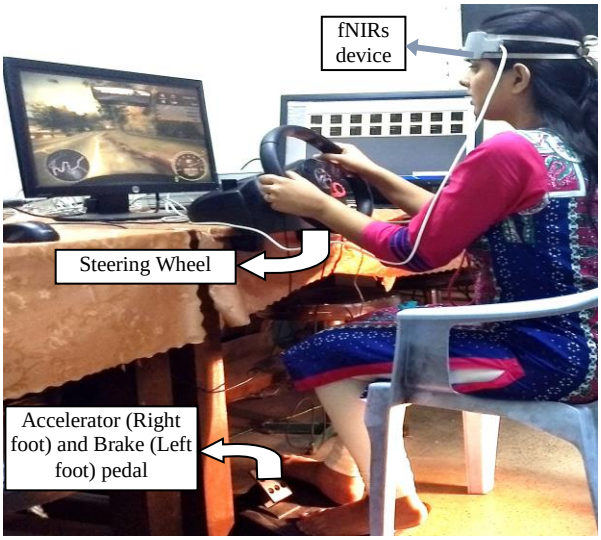

(a)

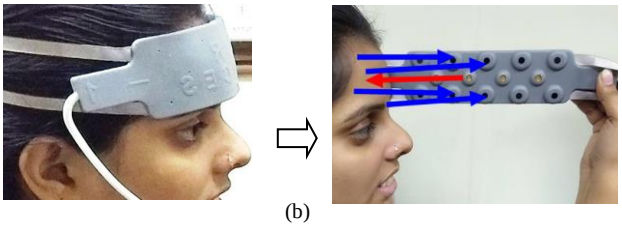

(b)

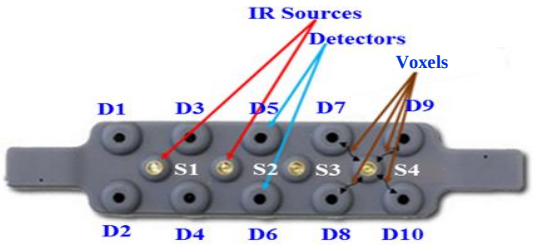

(c)

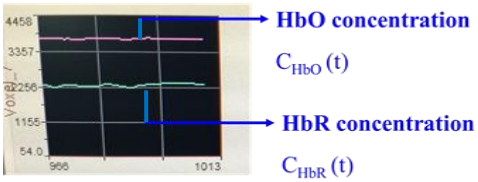

(d)

Fig. 7 (a) Experimental set-up with fNIRs data acquisition (b) IR penetration into the brain and its detection by the fNIRs device, (c) Structure of the fNIRs device (d) HbO and HbR concentration plot of a voxel

TABLE I
LIST OF STIMULI AND REQUIRED ACTIONS

S. No.	Type of stimulus	Required action
1	Making Right Turn	Steering Right
2	Making Left Turn	Steering Left
3	Bumper ahead	Brake

4	Side-car is too wide/ too close	Steering control
5	Front car speed decreases	Brake
6	Change in traffic signal	Acceleration/ Brake
7	Front car speed increases	Acceleration
8	Sharp turn in front	Steering control
9	U-turn	Steering control
10	Speed Control over bridge	Steering control

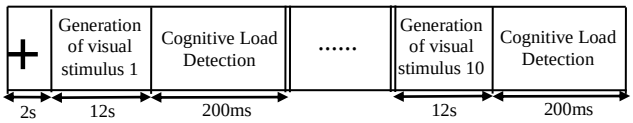

Fig. 8. Structure of the stimulus used with timing for online cognitive load detection

D. Experiment 1: Demonstration of decreasing Cognitive Load with increasing Learning Epochs for similar stimulus

The motivation of the present experiment is to estimate the cognitive load in motor-learning from the prefrontal activation. We here estimate and classify the cognitive load in 3 classes. It is noted that with increased learning epochs the cognitive load is decreasing. The same observation also follows from the measure of $diff_{avg}$ and also the topographic maps produced by the COBI studio software [41].

The above estimation is carried out over different learning epochs (LEs) for each of the 10 stimuli indicated above. Fig. 9 provides the $diff_{avg}$, the topographic maps and cognitive load classes obtained in three different LEs of making right and left turns (stimuli 1 and 2). Here, we confirm that the subject is able to learn to take left/right turns (LT/RT) efficiently from the gradual decrease in turning-angle Θ. Simultaneously, the peak of the $diff_{avg}$ along with computed cognitive load falls off gradually with repeated left/right turning and/or LEs. It is apparent from Fig. 9 that the first trial of learning incurs high cognitive load (symbolized in yellow), whereas the fifth trial for the same motor task yields medium cognitive load (symbolized in red). Lastly, the lowest activity (marked in blue) appears in the eighth trial of learning

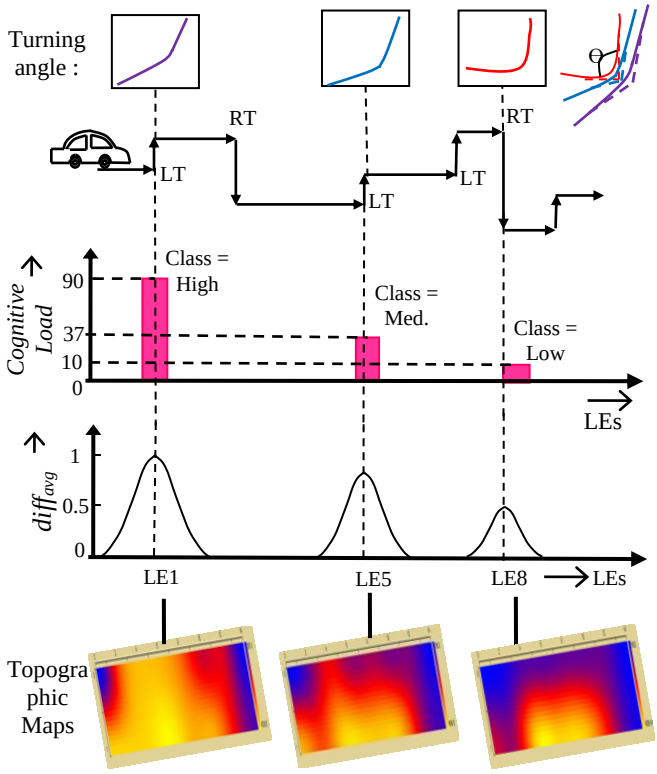

Fig. 9. The cognitive load, $diff_{avg}$ and the topographic maps obtained during the learning phase of left/right turning

resulting in low cognitive load. The decrease in cognitive load with increased learning epochs that follows up from this experiment is also supported by existing works [44].

E. Experiment 2: Automatic Extraction of discriminating fNIRs Features

We adopt two approaches for feature selection. First we obtain the 8 features out of 480 with an aim to maximize inter-class separation and minimize intra-class separation, which is done by minimizing (5). A cross-check of these 8 optimal features is also evident from the feature value plot (Fig. 10) for three classes. It is clear from the plot that the features F_{51} (Mean HbO conc. of voxel 3), F_{120} (Mean HbO conc. of voxel 6), F_{123} (Mean HbO conc. of voxel 8), F_{207} (Mean HbO conc. of voxel 16), F_{300} (avg. energy of voxel 5), F_{372} (avg. energy of voxel 12), F_{417} (avg. slope of voxel 5) and F_{471} (skewness of voxel 14) offer maximal inter-class separation.

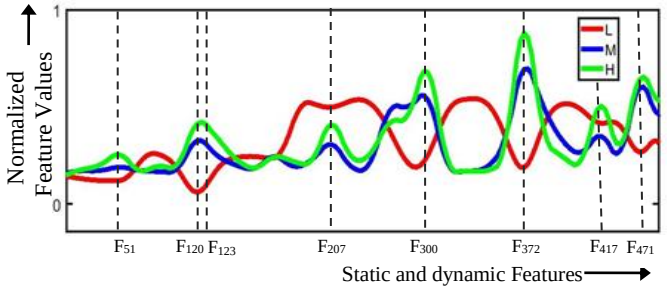

Fig. 10. Extracted fNIRs features to discriminate cognitive load of 3 classes. (The eight features, shown by the dotted line are most discriminating)

F. Experiment 3: Optimal Parameter Setting of Feature Selection and Classifier Units

Here, we use 2 DE-based optimizers, working in double loops. The inner loop is maintained by the left-cornered DE in Fig. 11, whereas the outer loop is maintained by the central DE. The left cornered DE is used to select the optimal features by minimizing (5) with a given value of η produced by the right DE

optimizer, used for parameter selection. For a given η, the left cornered DE on convergence produces the (tentative) best 8 out of 480 features by minimizing (5). These features are used by the GT2FS/IT2FS classifier for initializing the classifier parameters to produce class ${}^{i}Y$. The DE-based parameter selection then attempts to minimize

$$J = \sum_{\forall i} ({}^{i}Y_a - {}^{i}Y)^2, \tag{21}$$

subject to

$$\begin{aligned} &0.001 < \eta < 0.5, \\ &C_r^{Low} = C_l^{Med.}, \\ &C_r^{Med.} = C_l^{High}, \\ &0 < C_l^{Low} < C_r^{Low} \\ \text{and } &C_l^{High} < C_r^{High} \le 100. \end{aligned} \tag{22}$$

Here, ${}^{i}Y_a$ = actual class label of the *i*-the training instance and

${}^{i}Y$ = GT2FS classifier produced class label of the *i*-the training instance.

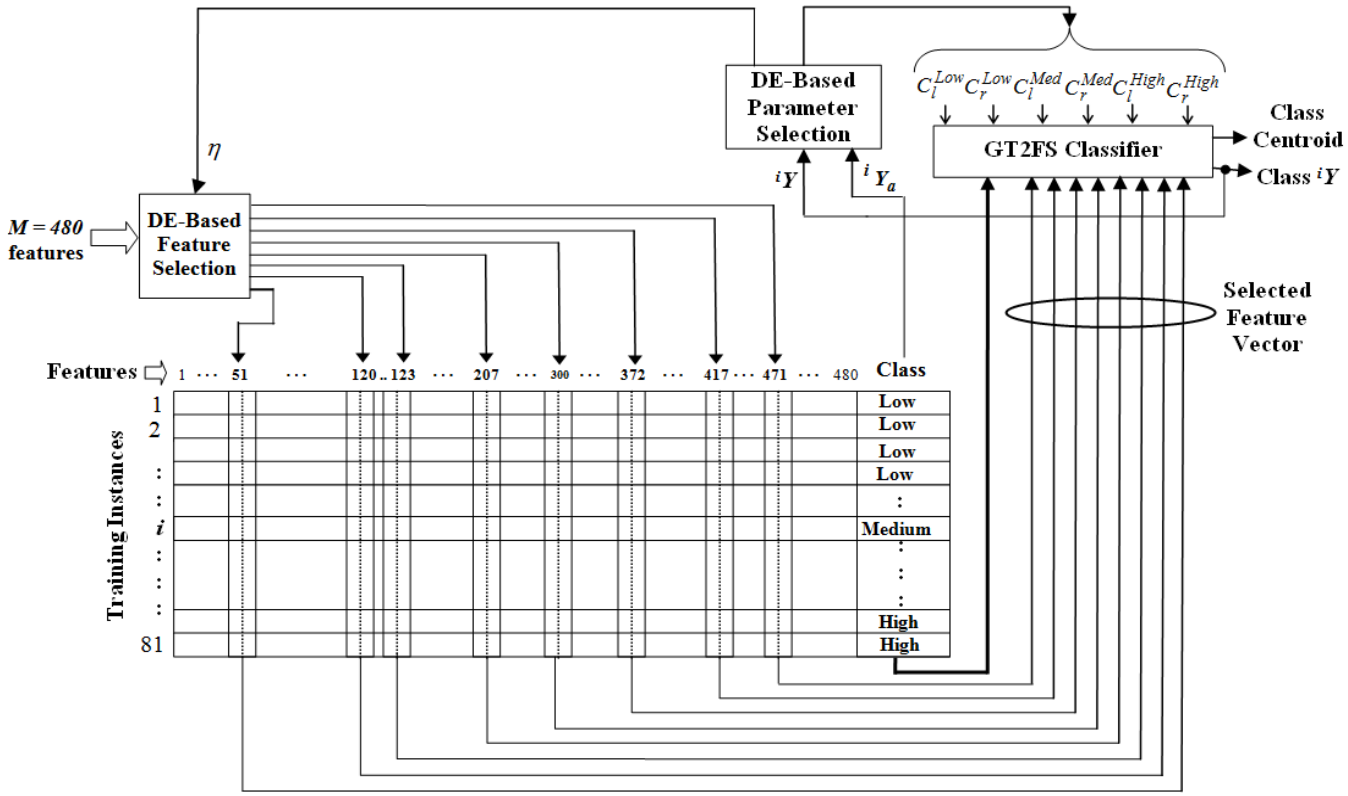

Fig. 11. Parameter selection of the GT2FS classifier for each healthy subject's 81 data-points of 480 dimensions

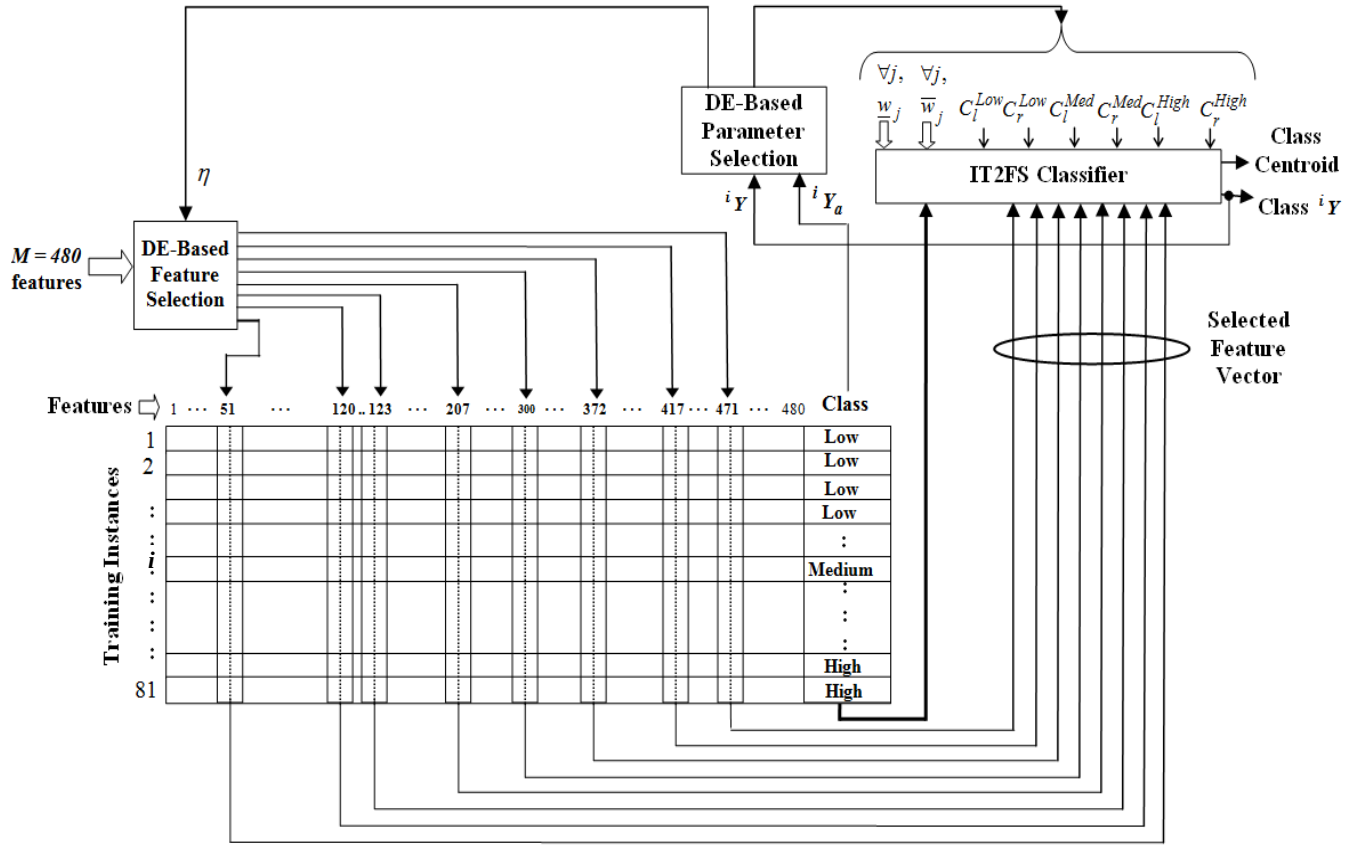

Fig. 12. Parameter selection of the IT2FS classifier for each healthy subject's 81 data-points of 480 dimension

The process explained above is repeated until both the DEs converge. Once converged, the η and classifier parameters $(C_l^{Low}, C_r^{Low}, C_l^{Med.}, C_r^{Med.}, C_l^{High} \text{ and } C_r^{High})$ are selected for online feature selection and classification. This is schematically illustrated in Fig. 11. The optimal parameters of GT2FS classifier and η are obtained as follows.

$$\eta = 0.0028,$$
$$C_l^{Low} = 7.16,\ C_r^{Low} = C_l^{Med.} = 24.22,\ C_r^{Med.} = C_l^{High} = 62.28$$
$$\text{and } C_r^{High} = 98.6.$$

In Fig. 12, we do the same for the IT2FS classifier. Here, we need to optimize $\underline{w}_j$ and $\overline{w}_j$ along with other classifier parameters $(C_l^{Low}, C_r^{Low}, C_l^{Med.}, C_r^{Med.}, C_l^{High} \text{ and } C_r^{High})$ and η. Here, we attempt to optimize (21),

subject to

$$0 \le \underline{w}_j \le \overline{w}_j \le 1,$$

other classifier parameter constraints,

and constraints on η, given in (22).

Fig. 12 explains the mechanism of the parameter selection for the IT2FS classifier and feature selection unit. After the parameters are obtained, we go for online classification of unknown input instances to classify the cognitive load into three classes: Low, Med. and High. The optimal values for the parameters of IT2FS classifier are listed below:

$$\eta = 0.00281,$$
$$C_l^{Low} = 7.72,\ C_r^{Low} = C_l^{Med.} = 24.01,\ C_r^{Med.} = C_l^{High} = 62.63$$
$$\text{and } C_r^{High} = 98.12,$$
$$\overline{w}_1 = 0.86,\ \underline{w}_1 = 0.20,\ \overline{w}_2 = 0.78,\ \underline{w}_2 = 0.12,\ \overline{w}_3 = 0.84,\ \underline{w}_3 = 0.12,\ \overline{w}_4 = 0.68,\ \underline{w}_4 = 0.42,\ \overline{w}_5 = 0.78,\ \underline{w}_5 = 0.32,\ \overline{w}_6 = 0.91,\ \underline{w}_6 = 0.18,$$
$$\overline{w}_7 = 0.84,\ \underline{w}_7 = 0.23,\ \overline{w}_8 = 0.97,\ \underline{w}_8 = 0.20,\ \overline{w}_9 = 0.86,\ \underline{w}_9 = 0.22,$$
$$\overline{w}_{10} = 0.90 \text{ and } \underline{w}_{10} = 0.12.$$

V. Biological Implications

The cognitive load distribution in prefrontal cortex (PFC) over the LEs is presented here by a voxel plot using MATLAB 2016 version. The mean of $CAR_\alpha(t)$ for α = 1 to 16 voxels are plotted as a 2 × 8 voxel plot demonstrating the 16 channels of the fNIRs system as shown in Fig. 13. The voxel plots indicate that 37 healthy subjects yield similar behavior in the activation pattern of PFC, irrespective of their age and gender. However, reduced dorsolateral PFC (DLPFC) activation associated with low learning ability is possibly related to improper growth/partial damage of the brain lobes [48], which we noticed in three Alzheimer's patients.

The following biological implications directly follow from the voxel plot of Fig. 13.

1. The left PFC has relatively higher activation than the right PFC when the subject experiences cognitive load in motor learning stimuli.
2. Fig. 13, depicting the regional response of the PFC, demonstrates that cognitive load shifts from the orbitofrontal cortex (OFC) to the ventro-lateral PFC (VLPFC) with increased LEs for healthy subjects. The brain anatomy responsible for OFC activation is associated with Broadmann area 11 (BA11), which has a significant involvement in reasoning, complex decision making, planning, and encoding new information into memory [45]-[47].
3. A significant reduction in the DLPFC activation is observed when cognitive load shifts from High to Low for the healthy subjects.
4. The OFC activation is reduced when the driving learner becomes an expert to drive safely in all road and traffic conditions. Thus, we conclude that initial learning trials need higher executive function and it is related to high cognitive load.

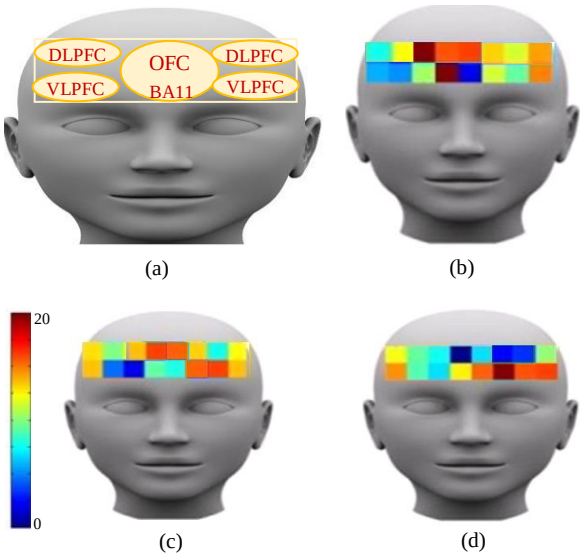

Fig.13 (a) Regions of the PFC; Voxel plot of the fNIRs data at (b) LE4 (Cognitive load: High), (c) LE10 (Cognitive Load: Med.) and (d) LE15 (Cognitive Load: Low) of subject no. 4

The graph shown in Fig. 14 also indicates that the cognitive load value (CLV) has a similar behavior with OFC activation for 3 different cognitive loads for the healthy subjects. The rest of the graphs are apparent and thus need no explanation.

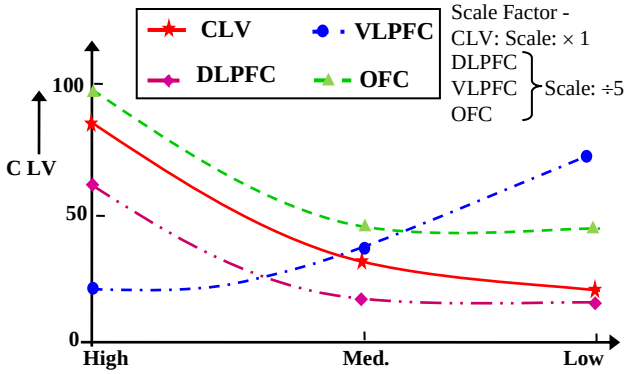

Fig.14. CLV variations in the prefrontal lobe with decreasing cognitive load

VI. Performance Analysis

This section provides experimental basis for performance analysis and comparison of the proposed classifiers with traditional/existing ones.

A. Performance Analysis of the proposed IT2FS and GT2FS classifier

To study the relative performance, we undertake three levels of analysis: i) classification accuracy, ii) run-time complexity of the classifiers and ii) joint occurrence of true (T)/false (F) and positive (P)/negative (N) cases. Table II contains the mean percentage classification accuracies of the proposed type-2 fuzzy classifiers against traditional fuzzy and non-fuzzy ones, including two existing GT2FS models [1] and [37], four existing IT2FS models [1], [50]-[52], evolving Type-2 Fuzzy Classifier (eT2Class) [29], Type-1 Fuzzy Neural Network [57], traditional type-1 Fuzzy set, SVM-RBF, LSVM, Linear Discriminant Analysis (LDA) [54] and *k*-Nearest Neighbor (kNN) [53]. In Table II, the percentage accuracy of each classifier is evaluated using (22), where *TP*, *TN*, *FP* and *FN* are the numbers of true positives, true negatives, false positives and false negatives respectively [37].

$$Classifier\ Accuracy = \frac{TP + TN}{TP + TN + FP + FN} \quad (22)$$

The experiment is accomplished with 11340 training instances for 37 healthy subjects and 3 brain-diseased subjects. Table II indicates that the proposed IT2FS and GT2FS classifiers outperform their nearest competitors by an average classification accuracy of ~ 1% and ~2% respectively.

TABLE II
MEAN PERCENTAGE CLASSIFICATION ACCURACY (STANDARD DEVIATION) OF PROPOSED CLASSIFIERS AGAINST STANDARD CLASSIFIERS FOR COGNITIVE LOAD DETECTION OF DRIVING LEARNERS

Classifiers	**No. of free parameters**	**Mean classifier accuracy in % (standard deviation)**		
		HIGH	**MED.**	**LOW**
Proposed GT2FS	**7**	**97.76 (0.0311)**	**95.94 (0.0123)**	**96.29 (0.0113)**
Proposed IT2FS	**27**	**96.29 (0.0104)**	**94.93 (0.0012)**	**95.23 (0.0127)**
SA-GT2FGG [37]	17	88.10 (0.0167)	85.14 (0.0231)	88.91 (0.1239)
GT2FS-NN [1]	1	93.16 (0.0921)	90.16 (0.0213)	91.26 (0.0134)
eT2Class [29]	33	94.12 (0.0121)	91.12 (0.0101)	93.12 (0.0211)
IT2FS-NN [1]	10	96.12 (0.0101)	94.16 (0.0216)	93.13 (0.0114)
McIT2FIS [50]	210	93.42 (0.0146)	90.89 (0.0215)	91.34 (0.0121)
ST2FNN [51]	172	91.95 (0.0112)	88.01 (0.0121)	88.17 (0.0129)
McIT2NFIS-RBE [52]	16	82.03 (0.0217)	80.03 (0.0215)	81.12 (0.0192)
Type 2 Fuzzy Set induced Classifier [22]	5	92.34 (0.0121)	91.56 (0.0109)	93.32 (0.0231)
Type 1 Fuzzy Set induced	3	90.17 (0.0112)	89.23 (0.0118)	90.71 (0.0121)

Classifier				
SVM-RBF	4	92.31 (0.0215)	91.19 (0.0291)	92.14 (0.0216)
LSVM	3	89.25 (0.0219)	86.93 (0.0214)	87.19 (0.0198)
LDA	3	89.72 (0.0211)	87.00 (0.0211)	80.11 (0.0181)
kNN	2	91.12 (0.0217)	90.11 (0.0201)	92.13 (0.0215)

Table III contains the run-times of the proposed type-2 classifiers against the traditional ones. The run-time complexity analysis of table III shows that our proposed IT2FS classifier algorithm requires the smallest run- time (~34 milliseconds) among all the classifiers and the proposed GT2FS classifier takes 94.23 milliseconds, which is also comparable to the run-time of the existing IT2FS classifiers, proposed in [50], [52].

TABLE III
RUN-TIME OF THE PROPOSED CLASSIFIERS AND OTHER COMPETITIVE CLASSIFIERS

Classifiers	**Run-time in HP Dual-core machine**
Proposed GT2FS	**94.23 ms**
Proposed IT2FS	**33.72 ms**
SA-GT2FGG [37]	98.18 ms
GT2FS-NN [1]	96.12 ms
eT2Class [29]	45.15 ms
IT2FS-NN [1]	38.22 ms
McIT2FIS [50]	95.18 ms
ST2FNN [51]	92.00 ms
McIT2NFIS-RBE [52]	100.4 ms
Type 2 Fuzzy Set induced Classifier [22]	48.94 ms
Type 1 Fuzzy Set induced Classifier	51.42 ms
SVM-RBF	40.12 ms
LSVM	35.98 ms
LDA	48.25 ms
kNN	35.11 ms

Finally, the relative performance of all the type-2 fuzzy classifiers, listed in Table IV, is compared by considering the 2 distinct classifier performance metrics: True Positive rate (TPR), and True Negative Rate (TNR) [37], given by (23) and (24). Here, GT2FS is found to outperform all existing and the proposed IT2FS classifier algorithm by around 1-3% of TPR value.

$$TPR = \frac{TP}{TP + FN} \times 100\% \tag{23}$$

$$TNR = \frac{TN}{TP + FN} \times 100\% \quad (24)$$

TABLE IV
COMPARATIVE STUDY OF PERCENTAGE TPR AND TNR OF THE PROPOSED CLASSIFIERS WITH EXISTING GT2FS AND IT2FS CLASSIFIERS

Classifier	**Performance Metrics**	
	TPR%	**TNR%**
GT2FS (proposed)	**98**	**96**
IT2FS (proposed)	**97**	**95**
SA-GT2FGG [37]	89	87
GT2FS-NN [1]	91.13	87.24
IT2FS-NN [1]	89.87	84.15
McIT2FS [50]	92.82	1.88
ST2FNN [51]	92.13	90.97
McIT2NFIS-RBE [52]	77.79	72.98

B. Statistical Validation of the classifier using McNemar's Test

We select McNemar's test [36] to compare the relative performance of the proposed DE-based feature selection induced GT2FS classifier with the other standard classifiers (Table VI). The statistical validation is performed with only one database prepared at Brain Imaging Laboratory of Jadavpur University. Most of the statistical tests [68] undertaken to compare classifier-performance require a large number of databases to determine the z-score metric used to accept/reject the null hypothesis (that all classifiers are equally good). Unfortunately, for the present experiment we prepared a single database, and so we use the McNemar's test, which requires a single database for statistical validation of the classifiers [36].

In Table V, **Z** indicates the probability of accepting/rejecting the null hypothesis, which indicates that all the classifiers are equally good. Table V confirms that the proposed GT2FS classifier is comparable with the proposed IT2FS classifier only.

TABLE V
STATISTICAL VALIDATION OF THE CLASSIFIERS USING MCNAMER'S TEST

Reference Algorithm: Proposed GT2FS Induced Classifier				
Classifier algorithm used for comparison using the 20 optimal features	**Parameters used for McNemar's Test**		**Z**	**Comments on acceptance / rejection of hypothesis**
	m	***n***		
Proposed IT2FS	5	14	3.684	**Accept**
SA-GT2FGG [37]	20	49	11.36	Reject
GT2FS-NN [1]	12	57	28.06	Reject

eT2Class [29]	13	36	9.877	Reject
IT2FS-NN [1]	22	45	7.223	Reject
McIT2FS [50]	7	18	4.OO	Reject
ST2FNN [51]	16	33	5.224	Reject
McIT2NFIS-RBE [52]	18	35	4.83	Reject
Type 2 Fuzzy Set induced Classifier	20	65	10.12	Reject
Type 1 Fuzzy Set induced Classifier	29	73	18.13	Reject
SVM-RBF	22	39	4.197	Reject
LSVM	15	33	6.021	Reject
LDA	17	67	28.58	Reject
kNN	19	39	6.224	Reject

VII. Conclusions

The paper proposes a novel approach to cognitive load assessment and classification of driving learners using an fNIRs device. A GT2FS induced classifier has been developed and tested over 37 healthy subjects and 3 brain patients using a laboratory model of a driving set-up. Experiments undertaken reveal that the proposed classifier outperforms its competitors by a large margin. A statistical test undertaken confirms the better classifying ability of the proposed GT2FS classifier over its competitors. The proposed system would have applications to identify people with high cognitive load for moderate/low traffic conditions, thereby saving people from having a psychological set-back/trauma due to tremendous mental pressure in high cognitive load. Biological implication of the research results is also narrated briefly here. It is apparent from the voxel plots that DLPFC and OFC are primarily engaged in HIGH cognitive load tasks. They are less influenced when the cognitive load is reduced. Determining the cognitive pathways in the brain during the learning phase of driving is another interesting and open problem. A detailed study of this using fNIRs alone is almost next to impossible. One approach to solve it perhaps is to compositely utilize both cortical signals by EEG or otherwise along with brain activation results obtained from fMRI and/or fNIRs devices.

Acknowledgment

The authors gratefully acknowledge the funding they received from the UPE-II Project in Cognitive Science offered by University Grants Commission (UGC) to Jadavpur University.

References

[1] A. Saha, A. Konar, and A. K. Nagar, "EEG Analysis for Cognitive Failure Detection in Driving Using Type-2 Fuzzy Classifiers." *IEEE Trans. Emerging Topics in Computational Intelligence* pp: 437-453, 2017.

[2] M. N. Murty, and V. S. Devi, *Pattern Recognition: An Algorithmic Approach*. Springer Science & Business Media, 2011.

[3] F. C. Lin, L. W. Ko, C. H. Chuang, T. P. Su, and C. T. Li, "Generalized EEG-based drowsiness prediction system by using a self-organizing neural fuzzy system." *IEEE Trans. Circuits and Systems* I, vol. 9, no. 9, pp: 2044-2055, 2012.

[4] A. Konar, *Cognitive engineering: a distributed approach to machine intelligence*. Springer, 2007.

[5] M. Matsui, K. Tanaka, M. Yonezawa, and M. Kurachi, "Activation of the prefrontal cortex during memory learning: Near-infrared spectroscopy study." *Psychi. and clinical neurosc. vol.* 61, pp: 31-38, 2007.

[6] Y. Ono, J. A. Noah, X. Zhang, Y. Nomoto, T. Suzuki, S. Shimada, A. Tachibana, S. Bronner, and J. Hirsch, "Motor learning and modulation of prefrontal cortex: an fNIRS assessment." *J. of Neural Engineering* 12, no. 6, 066004, 2015.

[7] T. Nguyen, A. Khosravi, D. Creighton and S. Nahavandi, "EEG signal classification for BCI applications by Wavelets and Interval Type-2 Fuzzy Logic System." *Expert Sys. Appl.*, vol. 42, no. 9, pp: 4370-4380, 2015.

[8] H. Boril, S. O. Sadjadi, T. Kleinschmidt, and J. H. Hansen, "Analysis and detection of cognitive load and frustration in drivers' speech." *Proc. of INTERSPEECH* 2010, pp: 502-505, 2010.

[9] K. R. Dixon, K. Hagemann, J. Basilico, C. Forsythe, S. Rothe, M. Schrauf, and W. E. Kincses, "Improved team performance using EEG-and context-based cognitive-state classifications for a vehicle crew." *Int. Conf. Foundations of Augmented Cognition*, pp. 365-372. Springer, Berlin, Heidelberg, 2009.

[10] R. S. Blumenfeld, and C. Ranganath, "Dorsolateral prefrontal cortex promotes long-term memory formation through its role in working memory organization." *J. of Neurosc.* 26, no. 3, pp: 916-925, 2006.

[11] V. M. Vogan, B. R. Morgan, W. Lee, T. L. Powell, M. L. Smith, and M. J. Taylor, "The neural correlates of visuo-spatial working memory in children with autism spectrum disorder: effects of cognitive load." *J. of neurodevelopmental disorders* 6, no. 1 pp: 19, 2014.

[12] A. De, A. Konar, A. Samanta, S. Biswas, A. L. Ralescu, and A. K. Nagar, "Cognitive load classification in learning tasks from hemodynamic responses using type-2 fuzzy sets." In Proc. of IEEE Int. Conf. on Fuzzy Systems (FUZZ-IEEE) 2017, pp. 1-6, 2017.

[13] M. Witte, M. Ninaus, S. E. Kober, C. Neuper, and G. Wood, "Neuronal correlates of cognitive control during gaming revealed by near-infrared spectroscopy." *PloS one*, 10(8), e0134816, 2015.

[14] F. Lu and Z. Yuan, "Cortical changes of hemodynamic signals during motor skill learning: a functional NIRS study," in *TENCON* 2015-2015 IEEE Region 10 Conference, 2015.

[15] A. C. Ehlis, C. G. Bähne, C. P. Jacob, M. J. Herrmann, and A. J. Fallgatter, "Reduced lateral prefrontal activation in adult patients with attention-deficit/hyperactivity disorder (ADHD) during a working memory task: a functional near-infrared spectroscopy (fNIRS) study." *J. of Psychiatric Research* 42, no. 13, pp: 1060-1067, 2008.

[16] A. Vermeij, A. H. E. A. van Beek, M. G. O. Rikkert,J. A. H. R. Claassen and R. P. Kessels, "Effects of Agingon Cerebral Oxygenation during Working-Memory Performance: A Functional Near-Infrared Spectroscopy Study," *Plos One*, p. e46210, 2012.

[17] L. Ferreri, J. J. Aucouturier, M. Muthalib, E. Bigand and A.Bugaiska, "Music improves verbal memory encoding while decreasing prefrontal cortex activity: an fNIRS study," *Frontiers in Human Neuroscience*, vol. 7, p. 779, 2013.

[18] Q. Ma, Y. Huang and L. Wang, "Left Prefrontal Activity Reflects the Ability of Vicarious Fear Learning: A Functional Near Infrared Spectroscopy Study," *The Scientific World J.*, p. Article ID 652542, 2013.

[19] M. Dan, A. Saha, A. Konar, A. L. Ralescu, and A. K. Nagar, "A type-2 fuzzy approach towards cognitive load detection using fNIRS signals." *In Proc. of IEEE Int. Conf. on Fuzzy Systems (FUZZ-IEEE*), pp. 2508-2515, 2016.

[20] P. A. Jackson and D. O. Kennedy, "The application of near infrared spectroscopy in nutritional intervention studies*." Frontiers in human neuroscience* 7 p:473, 2013.

[21] M. Pratama, J. Lu, E. Lughofer, G. Zhang and S. Anavatti, "Scaffolding type-2 classifier for incremental learning under concept drifts," *Neurocomputing*, vol. 191, pp.304-329, 2016.

[22] A. Halder, A. Konar, R. Mandal, A. Chakraborty, P. Bhowmik, N. R. Pal, and A. K. Nagar, "General and interval type-2 fuzzy face-space approach to emotion recognition." *IEEE Trans. Systems, Man, and Cybernetics: Systems* 43, no. 3 pp: 587-605, 2013.

[23] J. M. Mendel, R. I. John, and F. Liu, "Interval type-2 fuzzy logic systems made simple." *IEEE t Trans. fuzzy systems* 14, no. 6 pp: 808-821, 2006.

[24] C. Wagner, and H. Hagras, "Toward general type-2 fuzzy logic systems based on zSlices." *IEEE Trans. Fuzzy Systems* 18, no. 4 pp: 637-660, 2010.

[25] P. Manoilov, "EEG eye-blinking artefacts power spectrum analysis." *In Proceedings of the Int. Conf. on Computer Systems and Technologies-CompSysTech*'06, pp. 3-5. 2006.

[26] N. Naseer, and K. S. Hong, "fNIRS-based brain-computer interfaces: a review." *Frontiers in human neuroscience* 9, 2015.

[27] A. Hyvärinen, J. Karhunen, and E. Oja, *Independent component analysis*. John Wiley & Sons, vol. 46., 2004.

[28] C. Shen, Z. Cai, R. A. Maxion, G. Xiang, and X. Guan, "Comparing classification algorithm for mouse dynamics based user identification." *In Fifth Int. Conf. on Biometrics: Theory, Applications and Systems* (BTAS), pp. 61-66, IEEE, 2012.

[29] M. Pratama, J. Lu and G. Zhang, "Evolving Type-2 Fuzzy Classifier," *IEEE Trans. Fuzzy Systems*, vol. 24, no. 3, pp. 574-589, 2016.

[30] D. Wu and J. M. Mendel, "Enhanced karnik--mendel algorithms." *IEEE Trans. Fuzzy Systems* 17, vol. no. 4, pp: 923-934, 2009.

[31] N. N. Karnik and J. M. Mendel, "Centroid of a type-2 fuzzy set," *Information Sciences*, vol. 132, pp. 195–220, 2001.

[32] P. Rakshit, A. Konar, P. Bhowmik, I. Goswami, S. Das, L. C. Jain and A. K. Nagar, "Realization of an adaptive memetic algorithm using differential evolution and q-learning: a case study in multirobot path planning." *IEEE Trans. Systems, Man, and Cybernetics: Systems* 43, vol. no. 4, pp: 814-831, 2013.

[33] D. Wu, "A Constraint Representation Theorem for Interval Type-2 Fuzzy Sets Using Convex and Normal Embedded Type-1 Fuzzy Sets, and Its Application to Centroid Computation", in: *Proceedings of World Conference on Soft Computing*, San Francisco, CA, May 2011.

[34] D. Bhattacharya, A. Konar, and P. Das. "Secondary factor induced stock index time-series prediction using self-adaptive interval type-2 fuzzy sets." *Neurocomputing* 171 pp: 551-568, 2016.

[35] J. M. Mendel and R. I B. John, "Type-2 fuzzy sets made simple." *IEEE Trans. Fuzzy Systems* 10, vol. no. 2, pp: 117-127, 2002.

[36] T. G. Dietterich, "Approximate statistical tests for comparing supervised classification learning algorithms." *Neural computation* 10, no. 7 pp: 1895-1923, 1998.

[37] J. Andreu-Perez, F. Cao, H. Hagras and G. Z. Yang, "A Self-Adaptive Online Brain Machine Interface of a Humanoid Robot through a General Type-2 Fuzzy Inference System," *IEEE Trans. Fuzzy Systems*, no. 99, 2016.

[38] G. J. Klir and B. Yuan, *Fuzzy Sets and Fuzzy Logic: Theory and Applications*, Pretice-Hall, 1997.

[39] G. Durantin, F.Dehais, and A. Delorme, "Characterization of mind wandering using fNIRS." *Frontiers in systems neuroscience* 9, 2015.

[40] R.Vega, A. G. Hernandez-Reynoso, E. K. Linn, R. Q. Fuentes-Aguilar, G. Sanchez-Ante, A. Santos-Garcia, and A. Garcia-Gonzalez, "Hemodynamic pattern recognition during deception process using functional near-infrared spectroscopy." *J. of medical and biological engineering* 36, no. 1 pp: 22-31, 2016.

[41] G. Aranyi, F. Pecune, F. Charles, C. Pelachaud, and M. Cavazza, "Affective interaction with a virtual character through an fNIRS brain-computer interface." *Frontiers in computational neuroscience* 10, 2016.

[42] W. Pedrycz, *Fuzzy sets engineering*. CRC press, 1995.

[43] J. Mendel, and D. Wu, *Perceptual computing: Aiding people in making subjective judgments*. vol. 13. John Wiley & Sons, 2010.

[44] T. Liu, H. Saito, and M. Oi, "Distinctive activation patterns under intrinsically versus extrinsically driven cognitive loads in prefrontal cortex: a near-infrared spectroscopy study using a driving video game." *Neuroscience letters* 506, no. 2 pp: 220-224, 2012.

[45] R. D. Rogers, A. M. Owen, H. C. Middleton, E. J. Williams, J. D. Pickard, B. J. Sahakian and T. W. Robbins, ”Choosing between small, likely rewards and large, unlikely rewards activates inferior and orbital prefrontal cortex,” *The J. of Neuroscience*, pp. 9029-9038, 1999.

[46] S. Frey and M. Petrides, “Orbitofrontal cortex: A key prefrontal region for encoding information,” *PNAS*, pp. 8723-8727, 2000.

[47] A. K. Barbey, M. Koening and J. Grafman, ”Dorsolateral prefrontal contributions in human working memory,” *Cortex*, vol. 49, pp. 1195-1205, 2013.

[48] T. G. Lee, R. S. Blumenfeld and M. dEsposito, ”Disruption of Dorsolateral but Not Ventrolateral Prefrontal Cortex Improves Unconscious Perceptual Memories,” *J. of Neuroscience*, vol. 33, pp. 13233-13237, 2013.

[49] S. Das, A. Abraham, and A. Konar, “Automatic clustering using an improved differential evolution algorithm,” *IEEE Trans. Systems, Man, and Cybernetics-Part A: Systems and Humans*, vol. 38, no. 1, pp. 218-237, 2008.

[50] A. K. Das, K. Subramanian and S. Sundaram, “An Evolving Interval Type-2 Neurofuzzy Inference System and Its Metacognitive Sequential Learning Algorithm,” *IEEE Trans. Fuzzy Systems*, vol. 23, no. 6, pp. 2080-2093, 2015.

[51] C. M. Lin, Y. M. Chen and C. S. Hsueh, “A self-organizing interval type-2 fuzzy neural network for radar emitter identification,” *Int. J. Fuzzy Syst*, vol. 16, no. 1 pp. 20-30, 2014.

[52] A. K. Das, S. Suresh, N. Sundararajan, and K. Subramanian, "A subject specific frequency band selection for efficient BCI-an interval type-2fuzzy inference system approach," *in Proceedings of the IEEE* Int. Conf. *on Fuzzy Systems*, pp. 1-8, 2015.

[53] M. L. Zhang, and Z. H. Zhou, "A k-nearest neighbor based algorithm for multi-label classification." *In Granular Computing*, IEEE Int. Conf. on, vol. 2, pp. 718-721. IEEE, 2005.

[54] S. Pang, S. Ozawa, and N. Kasabov, "Incremental linear discriminant analysis for classification of data streams." *IEEE Trans. Systems, Man, and Cybernetics*, Part B (Cybernetics) 35, no. 5 pp: 905-914, 2005.

[55] Z. Fu, A. Robles-Kelly and J. Zhou, "Mixing linear SVMs for nonlinear classification." *IEEE Trans. Neural Networks* 21, no. 12, pp: 1963-1975, 2010.

[56] B. C. Kuo, H. H. Ho, C. H. Li, C. C. Hung, and J. S. Taur, "A kernel-based feature selection method for SVM with RBF kernel for hyper spectral image classification." *IEEE J. of Selected Topics in Applied Earth Observations and Remote Sensing* 7, no. 1, pp:317-326, 2014.

[57] D. Baruah, P. Angelov, and J. Andreu, "Simpl_eClass: simplified potential-free evolving fuzzy rule-based classifiers," *In Proc. of IEEE Int. Conf. on Systems, Man, and Cybernetics (SMC)*, 2011 IEEE Int. Conf. on, pp.2249-2254, 2011.

[58] H. Zhao, P. C. Yuen, and J. T. Kwok, "A novel incremental principal component analysis and its application for face recognition," *IEEE Trans. Syst., Man, Cybern. B, Cybern.*, vol. 36, no. 4, pp. 873–886, Aug. 2006.

[59] P. Samanta, D. Bhattacharya, A. De, L. Ghosh, and A. Konar, "Music-Induced Emotion Classification from the Prefrontal Hemodynamics." In Int. Conf. *on Pattern Recognition and Machine Intelligence*, pp. 289-295. Springer, 2017.

[60] J. M. Mendel, "General type-2 fuzzy logic systems made simple: a tutorial." *IEEE Trans. Fuzzy Systems* 22, no. 5, pp: 1162-1182, 2014.

[61] K. Price, R. M. Storn, and J. A. Lampinen, *Differential evolution: a practical approach to global optimization*. Springer Science & Business Media, 2006.

[62] S. Das, and P. N. Suganthan, "Differential evolution: A survey of the state-of-the-art." *IEEE Trans. Evolutionary computation* 15, vol. no. 1, pp: 4-31, 2011.

[63] J. Tang, S. Alelyani, and H. Liu, "Feature selection for classification: A review." *Data Classification: Algorithms and Applications,p.* 37, 2014.

[64] Z. M. Hira, and D. F. Gillies. "A review of feature selection and feature extraction methods applied on microarray data." *Advances in bioinformatics*, 2015.

[65] K. Deb, A. Pratap, S. Agarwal, and T. A. M. T. Meyarivan, "A fast and elitist multiobjective genetic algorithm: NSGA-II." *IEEE Trans. Evolutionary Computation* 6, vol. no. 2, pp. 182-197, 2002.

[66] D. Wu, "Approaches for reducing the computational cost of interval type-2 fuzzy logic systems: overview and comparisons." *IEEE Trans. Fuzzy Systems* 21, vol. no. 1, pp: 80-99, 2013.

[67] S. Chakraborty, A. Konar, A. Ralescu, and N. R. Pal, "A fast algorithm to compute precise type-2 centroids for real-time control applications." *IEEE Trans. Cybernetics* 45, vol. no. 2, pp: 340-353, 2015.

[68] J. Demšar, "Statistical comparisons of classifiers over multiple data sets," *J. of Machine Learning Research*, vol. *7*, pp.1-30, 2006.

[69] fNIRs data for cognitive load assessment and classification, prepared at Artificial Intelligence Lab., ETCE Dept., Jadavpur University. See: http://amitkonar.com/tetci/howtoreaddata.pdf; http://amitkonar.com/tetci/fnirsdataload.zip .

Lidia Ghosh received her B.E. degree in Electronics and Tele-Communication Engineering from Bengal Institute of Technology, Techno India College in 2011, and her M. Tech. degree in Intelligent Automation and Robotics (IAR) from the department of Electronics and Tele-Communication Engineering, Jadavpur University, Kolkata in 2015. She was awarded Gold Medals for securing the highest percentage of marks in M. Tech in IAR in 2015. She is currently pursuing her Ph.D. in Cognitive Intelligence in Jadavpur University under the guidance of Prof. Amit Konar and Dr. Pratyusha Rakshit. Her current research interest includes human memory formation, short and long term memory interactions, and biological basis of perception and scientific creativity.

Amit Konar (SM' 2010) is currently a Professor in the department of Electronics and Tele-Communication Engineering, Jadavpur University, Kolkata, India. He earned his B.E. degree from Bengal Engineering College, Sibpur in 1983, and his M.E., M. Phil. and Ph.D. degrees, all from Jadavpur University in 1985, 1988 and 2004 respectively. Dr. Konar has

published 15 books and over 350 research papers in leading international journals and conference proceeding. He has supervised 28 PhD theses and 262 Masters' theses. He is a recipient of AICTE-accredited Career Award for Young Teachers for the period: 1997-2000. He is nominated as a Fellow of West Bengal Academy of Science and Engineering in 2010 and (Indian) National Academy of Engineering in 2015. Dr. Konar has been serving as an Associate Editor of several international journals, including IEEE Transactions of Fuzzy Systems and IEEE Transactions of Emerging Trends in Computational Intelligence. His current research interest includes Cognitive Neuroscience, Brain-Computer Interfaces, Type-2 Fuzzy Sets and Multi-agent Systems.

Dr. Pratyusha Rakshit received the B. Tech degree in Electronics and Communication Engineering (ECE) from Institute of Engineering and Management, India, and M.E. degree in Control Engineering from Electronics and Telecommunication Engineering (ETCE) Department, Jadavpur University, India in 2010 and 2012 respectively. She was awarded her Ph.D. (Engineering) degree from Jadavpur University, India in 2016. From August 2015 to November 2015, she was an Assistant Professor in ETCE Department, Indian Institute of Engineering Science and Technology, India. She is currently an Assistant Professor in ETCE Department, Jadavpur University. She was awarded Gold Medals for securing the highest percentage of marks in B. Tech in ECE and among all the courses of M.E. respectively in 2010 and 2012. She was the recipient of CSIR Senior Research Fellowship, INSPIRE Fellowship and UGC UPE-II Junior Research Fellowship. Her principal research interests include artificial and computational intelligence, evolutionary computation, robotics, bioinformatics, pattern recognition, fuzzy logic, cognitive science and human-computer interaction. She is an author of over 50 papers published in top international journals and conference proceedings. She serves as a reviewer in IEEE-TFS, IEEE-SMC: Systems, Neurocomputing, Information Sciences, and Applied Soft Computing.

Atulya K. Nagar received the D.Phil. degree in applied nonlinear mathematics from the University of York, York, U.K., in 1996. He is a Professor of mathematical sciences at Liverpool Hope University, Liverpool, U.K., where he is the Dean of the Faculty of Science. He received a prestigious Commonwealth Fellowship for the D.Phil. degree. His research interests include nonlinear mathematics, natural computing, and systems engineering. He is the Editor-in-Chief of International Journal of Artificial Intelligence and Soft Computing and serves on the editorial boards for a number of prestigious journals, including the Journal of Universal Computer Science. He was the Conference General Chair and member of the International Program Committee for several international conferences and was invited to deliver keynote lectures at a number of such forums.